International Journal of Scientific Engineering and Applied Science (IJSEAS) – Volume-6, Issue-11, November 2020
ISSN: 2395-3470
www.ijseas.com

Label-free Biomarker Detection of Diet Induced Murine Liver Diseases and Evaluation Using Raman Spectroscopy

Valpapuram Immanuel[1], Pushparani MichealRaj[2], Natalia Malara[1], Maria Laura Coluccio[2], Vincenzo Mollace[1]

[1] Department of Health Sciences, University "Magna Græcia" of Catanzaro, Italy

[2] Bionem Laboratory, Department of Experimental and Clinical Medicine University "Magna Græcia" of Catanzaro, Italy

Abstract

The present study is minimally-invasive in nature as Raman finger prints provide a validation that highlights the sensitivity of label-free Raman spectroscopy at ultra-low concentration and indicate the potential to predict murine liver fibrosis. Here, we analyzed three sets of murine liver tissues samples, of which one is pre-treated control (CTR) and two are post-treated samples vehicle (VC) and Bergamot (BPF), to probe Raman spectroscopic tissue assessments. The results of our studies reveal an unprecedented difference in lipid, protein and collagen content between the pre- and post-treated liver tissue. There is also a possibility of sensitive detection of vitamin A. Our data provide relatively simple analytical approach i.e Raman spectroscopy on murine liver tissue enables fast quantification of murine liver fibrosis and as such is a potential diagnostic method in clinical research.

Keywords: *Raman spectroscopy, Biomarker, murine liver fibrosis, label-free, biomolecules*

1. Introduction

Over the last two decades, Raman spectroscopy studies for biological and clinical evaluation have formulated precise, supersensitive and promising analytical technique, e.g. liver fibrosis, cancer, liver infectious diseases, regenerative medicine and more [1-3]. Raman spectroscopy represents a viable methodology, this technique relies on the analysis of light spontaneously scattered from the specimen allowing for chemical compound assessment. From the scattered spectrum, it is possible to extract chemical information associated with vibrational modes of molecules present in the sample. Indeed, each molecule shows up unique Raman spectrum so that a specific fingerprint can be associated with each biological substance, a fact that is of fundamental importance to establish the specificity of analysis methods. Unlike many other analytical techniques, Raman spectroscopy allows label-free, minimally-invasive analysis of samples and it is compatible with measurements in aqueous solution, indispensable conditions for reducing the biological sample pretreatment [4-6].

Raman spectroscopy is a simple laser technique for direct detection of sub-molecular level information, allowing investigation on functional groups, bonding types, and molecular conformations. This vibrational technique is simple, reproducible and non-destructive to the tissue. The technique is an inelastic scattering of photons on molecule bond vibrations names as Raman scattering, these spectral bands in vibrational spectra are molecule specific and provide direct information about the biochemical composition [7, 8]. These bands are relatively narrow, easy to resolve, and sensitive to molecular structure, conformation, and environment, because a small fraction of photons approximately of the order of 10^8 are in-elastically scattered and energy loss to the molecular bond vibration. Hence, the difference in the energy between the incident and scattered photons corresponds to the energy to excite or de-excite the molecular vibration.

Once the scattered photon is captured, that results in a spectrum of narrow peaks and assigns to a specific vibrational resonance of a molecular group. For this reason, only micrograms of samples are required. Each Raman peak of a particular molecular vibration occurs at a specific vibrational energy relative to the wavelength of excitation source, which is displayed as a “Raman shift” in units of

"wavenumbers" (in cm^{-1}). Therefore, a Raman spectrum resembles a "molecular fingerprint" of the sample under investigation [9].

The aim of this study is to investigate murine liver fibrosis and associated disorders. Liver fibrosis is caused by numerous liver-impairing agents and hepatotoxic drugs. In case of continuous damage by agents results in liver fibrosis, cirrhosis. Each time a Liver is afflicted by such detrimental agents, it tries to repair itself, but the liver damage done by cirrhosis generally cannot be undone [10]. If liver fibrosis or cirrhosis is diagnosed early and the cause is treated, further deterioration can be controlled. Hence, it is grabbing more attention for early diagnosis, the advantage of early detection and diagnosis of fibrosis is ensuring to prevent and development of cirrhosis [11, 12].

In order to answer the early diagnosis of murine liver fibrosis and to prevent, we characterized the behavior of pre-treated murine liver tissue (CTR) and post-treated murine tissue (VC and BPF) under Raman spectroscopy. When subjected to analysis of murine liver tissue, Raman spectroscopy provides information of molecular composition of tissues. In addition, since a molecular vibration is sensitive to its neighboring molecular bonds and molecular structure, Raman spectroscopy also provides information about the conformation of biomolecules and their interactions. It is strongly believed that in spectroscopy techniques, both the reliable experimental procedure and characterization of spectral peak position, their assignment along with accurate peak detection and definition are of crucial importance [13]. The spectral interpretation investigations are reported in the present study for murine liver tissue which provided a detailed account of spectral frequencies of the murine Liver tissues and intend to measure differences between pre-treated and post-treated samples. In addition, Raman signatures revealed significant and reliable differences in lipid, protein and collagen in the investigated murine liver tissues [14-16]. There is also a possibility of sensitive detection of vitamin A, lipid and Collagen which could be detected by Raman spectroscopy for early diagnosis of murine liver fibrosis. There are other viable appearances of proline and tyrosine [17]. We also observed random intensity differences in the peaks corresponding to one or all of the biomolecules. The increase and decrease of peaks are caused by amino acids, nucleic acids, proline and glucose. The characteristic of the disordered intensity shifts of peaks indicates biomolecule composition changes in the murine liver tissue. Further, a considerable increase of the collagen, lipids and protein content possibly with a high-fat diet and serve samples of fibrosis. Also, the more drastic change caused is significant not only with collagen increase or lipids but also with protein accumulation alongside significant loss of vitamin A content. The murine liver tissue analysis based on average Raman spectra recorder in the present study provide highly sensitive and specificity of slight and drastic changes in the post-treated and control murine liver tissue [18].

The present study is minimally-invasive in nature as Raman finger printings provide a validation that highlight the sensitivity of label-free Raman spectroscopy and indicate the competence to predict liver fibrosis, therefore it is a potential and useful diagnostic tool, relatively simple analytical approach to predict murine liver fibrosis.

2. Materials and Methods

2.1 Sample Extraction, purification and Sample Preparation

The samples are received in various pre-conditions as follows: Arm 1 is CTR1 and CTR2 – Normal Food and Tap water. Arm 2 is VC4 and VC5 – Fat food, sugar water + normal water by gavage. Arm 3 is BPF7 and BPF8 – BPF powder + water + fat food + sugar water. In order to obtain optimal results, the samples are provided with a buffer solution (LYSIS), Lysis Buffer Formula, 150 mM NaCl, 0.1% TRITON, and 0.5% Sodium Deoxycholate, 0.1% SDS, 50mM TRIS-HCl pH 8, Inhibitor Protease, and Inhibitor Phosphatase. Once the sample is delivered with the Buffer solution, it is cryopreserved at -80°C. When the experiment is ready to be done, the samples are removed from cryopreservation, thawed and analysis is carried out at RT (room temperature). The length of each analysis is ensured to be under 20 minutes since the samples may succumb to death after this time [19].

2.2 Raman Experiments

In the present study, Raman spectroscopy used to optically probe to investigate the molecular changes associated with diseased tissues. The measurement of Raman scattered radiation, provides information on chemical bonding and molecular structure through the detection of photons that are scattered inelastically from a liver tissue using Laser wavelength 830nm (is ideal for biological samples). When the energy of incident photon is unaltered after collision with a liver tissue, the scattered photon has the same frequency as the incident photon, this phenomenon is Rayleigh or elastic scattering, but then again, 1 in 10^{10} million photon a very small portion can get scattered. The loss (or gain) in the photon energies corresponds to the difference in the final and initial vibrational energy levels of the molecules participating in the interaction. If the proton has a higher frequency and therefore lower energy than the incident light, this phenomenon is Stokes-Raman Scattering and is due to the change in vibrational mode of the sample, if it is higher, it is Anti-Stokes Raman Scattering[20]. At room temperatures, the Stokes Raman scattering process is predominant and Raman spectra is a plot of scattered intensity as a function of the energy difference between the incident and Raman scattered photons is equivalent to the frequency of the vibrational energy levels of the molecules participating in the interaction (Fig 1g). Consequently, the Raman spectra are characterized by shifts in wavenumbers or inverse of wavelength in cm^{-1} that are from the incident frequency. Accordingly, the frequency difference between incident and Raman-scattered light is labelled "Raman shift" is unique for any individual molecules that are measured by the detectors and characterized as 1/cm. Every molecule has a unique Raman spectrum are narrow, signifies the vibration of exact chemical bond or a single functional group in the molecule, also known as Raman "fingerprint".

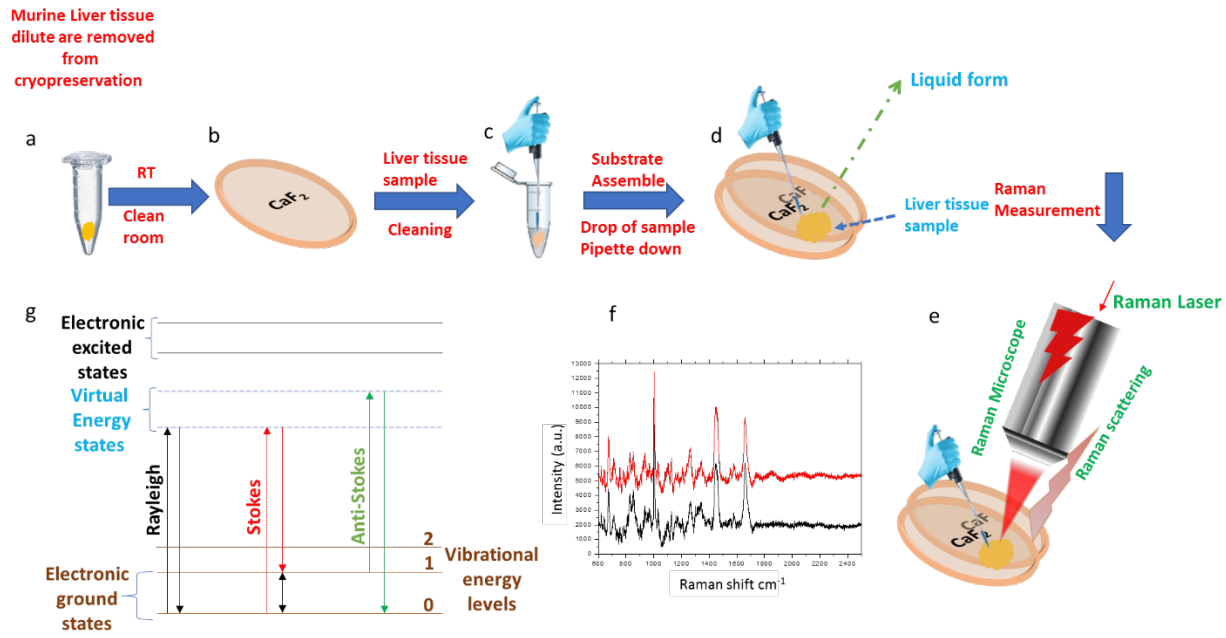

Figure 1: Raman Investigation Pattern a-g. a) Diluted murine liver tissue thawed to RT from cryopreservation; b) Cleaned CaF_2 coverslips first with Ethanol followed by DI wash and dried with N_2 gun, CaF_2 is used because of their excellent optical properties and negligible Raman spectra; c) Diluted samples of 1µL is pipetted over a CaF_2 coverslip; d) Assembled manually the top layer with another CaF_2 coverslip and the samples are correctly aligned between the sandwiched CaF_2 layers; e) The samples are excited with Raman spectrometer of 830nm and power 50mW; f) Raman spectra obtained for the aqueous medium of samples with limited noise; g) Schematic illustration of Raman and Rayleigh scattering. In Rayleigh and Raman scattering, the incident photon has much higher frequency whereas, the scattered photon is similar to incident in Rayleigh but a lower or higher frequency in Raman. This difference in frequency is interpreted as the molecular vibrational frequency that relates for any spectroscopic studies

To obtain high precision spectra, we ensured that we use the optimal procedure to acquire Raman spectra. Murine liver tissue thawed to Room Temperature (RT) from cryopreservation, the sample with buffer solution are sandwiched between two (Fig 1d) layers of CaF_2 (Calcium Fluoride), since CaF_2 has high optical properties against negligible Raman signals, Samples of 1 µl (Fig 1e) are then carefully handled to be pipetted on top of the lower CaF_2 glass and then top layer of CaF_2 glass is placed with utmost care not to disturb the sample. The Raman spectra of the murine liver tissues were obtained by the inVia Renishaw Raman microscopes with excitation laser wavelength of 830nm, the 50Lx objective (Olympus), the maximum laser power at the sample position 50mW was applied for acquisition of single spectra with 10 scans with an integration time of 10s. Each spectrum acquired in dark ambiance in order to avoid other light interaction on sample, Raman microspectrometer able to produce most of the finest spectra and with less noise (Fig 1f).

3. Results and Discussion

The full range (600-2500cm-1) of the Raman spectra was used for each spectra acquisition. The data is kept for analysis, including pre-processing by removal of cosmic ray, baseline, first derivative, second derivative, normalization, smoothing, and background correction and buffer subtraction to achieve optimal spectra. The Raman spectra are acquired for all sample variations in aqueous medium of CTR, VC and BPF were collected and are shown in Fig 2. Proteins, lipids, and collagen reflects specific fingerprint spectra. In present study, murine liver shows diverse functions as normal liver does which is critical for liver functions in terms of metabolism of lipids, protein functions (collagen), storage of vitamin A, and other minerals [16]. With these diverse functions reflected in building of various cells that are involved in the network of building organs such as hepatocytes, Hepatic Stellate Cells etc [21]. Having complex multitude liver functions, it is a key organ in the pathogenesis of many diseases. The Raman spectra shown in the present study is useful for the investigation and the role of protein, lipid and collagen variance in the murine liver tissue particular interest on the context liver fibrosis. Multiple peaks varying from weak to medium and strong to prominent are observed at different wavelengths and the spectral profile of individual murine tissue sample is significantly different depending on saturation, liquid state and geometrical isomerism [9].

Typical characteristic features of Raman spectra are discussed, there are multiple peaks varying for weak to medium and strong to prominent are observed at different wavelengths and summarized.

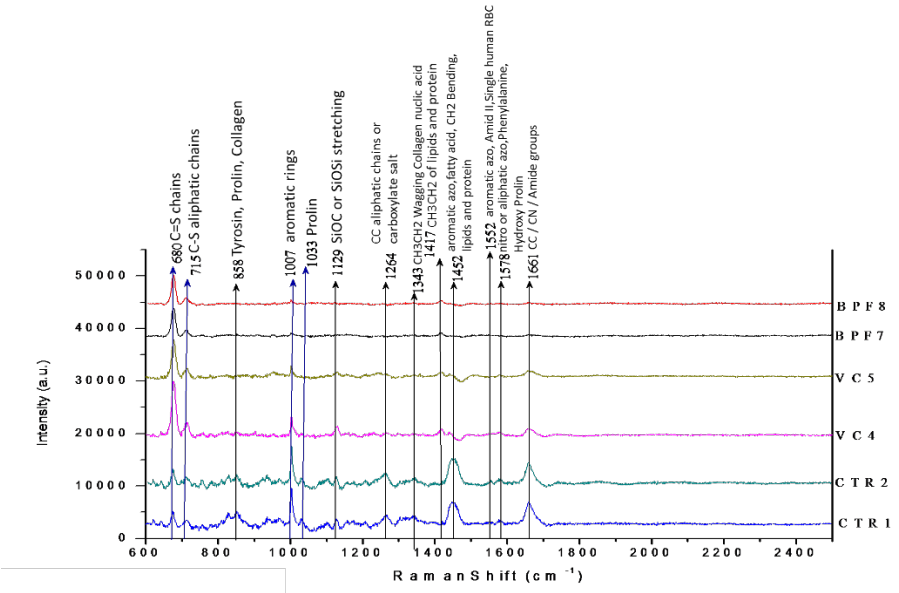

Figure 2: Raman spectra of Murine liver tissue acquired.

3.1 Peak assignments

Strong to Medium & Weak, All the samples have multiple similar signals of which most commonly found are 680, 715, 1007 and 1417 cm^{-1}. These peaks correspond to C=S chains, C-S aliphatic chains, aromatic rings and CH3CH2 of lipids & proteins respectively, at 680 cm^{-1} more pronounced in VC4 & VC5; strong in BPF7 & BPF8; whereas they are medium in CTR1 & CTR2, at 715 cm^{-1} medium in VC4 and VC5; weak in BPF7, BPF8, CTR1 and CTR2, 1007 cm^{-1} more pronounced in CTR1 & CTR2; strong in VC4; medium in VC5; whereas diminishing in BPF7 & BPF8, 1417 cm^{-1} diminishing in CTR1 and CTR2; weak in VC4, VC5, BPF7 and BPF8, Medium to diminishing. The peak at 1661 cm^{-1} is due to CC CN Amide groups, Lipids C55 C stretch. It seems to observe a medium intensity with CTR1 & CTR2, whereas with VC4 &VC5 they are weak, and no significant peak is observed on BPF samples. A peak at 858 cm^{-1} are due to presence of Tyrosine, Proline, Collagen, medium in VC4 & VC5; weak in CTR and BPF samples. Weak to diminishing, in addition to the above-mentioned signals and peaks, there are also other peaks with lesser intensity are observed with greater significance on the chemical substances used on the samples. It is summarized as below. At 1033 cm^{-1} due to Proline is weak in CTR1 & CTR2 whereas no signal observed in VC & BPF samples, At 1129 cm^{-1} due to Si-O-C or Si-O-Si stretching is weak in CTR1, CTR2 & VC4; whereas a little bump in VC5 and no signal in BPF samples, At 1264 cm^{-1} due to CC aliphatic chains or carboxylate salt is a weak peak found only in CTR1 1 & CTR2 samples, At 1343 cm^{-1} due to CH3CH2 wagging, collagen, nucleic acids are a feeble or diminishing peak present only in CTR samples, At 1552 cm^{-1} due to aromatic azo, Amide II groups, single human RBC is diminishing peak in CTR samples only, At 1578 cm^{-1} due to nitro or aliphatic azo, phenylalanine, hydroxyproline results in a weak peak at CTR samples only and a small bump in VC samples [17] (Fig 2).

Table1: Peak position and tentative assignments of Raman fingerprints for liver murine tissue [16, 22, 23]

Peak position in cm^{-1}	**Assignments**	**CTR**	**VC**	**BPF**
623	C=S Chain, C-C twisting (protein), C-C twist aromatic ring (one of C-C vibrations to be expected in aromatic structure of xylene), C-C twisting mode of phenylalanine (proteins), Cholesterol/Cholesterol esters	W	N/A or VW	N/A or VW
644	(C-S) gauche (aminoacid methionine), C-C twisting mode of tyrosine, C-C twisting mode of phenylalanine (proteins, C-C twisting mode of tyrosine)	W	VW	N/A
680	Ring breathing modes in the DNA bases, G (ring breathing modes in the DNA bases)/C-20- endo-anti heme	M	S	P
716	C-N (membrane phospholipids head)/adenine, CN2(CH3)3 (lipids), Choline group, C-N (membrane phospholipid head)/nucleotide peak, Symmetric stretch vibration of choline group, characteristic for phospholipids, Phosphatidylcholine, sphingomyelin, C-C-N symmetric stretching in phosphatidylcholine (lipid assignment), DNA, Cholesterol v(steroid ring) 720(w) Phospholipids	W	M	M
824	Out-of-plane ring breathing, tyrosine (protein assignment), Phosphodiester	M	VW	VW
854	Ring breathing mode of tyrosine & C-C stretch of proline ring, Glycogen, (C-O-C) skeletal mode of a-anomers (polysaccharides, pectin), Ring breathing tyrosine (proteins), Proline, tyrosine, (C-C), proline (CCH) ring breathing, tyrosine (protein assignment and	M	VW	VW

	polysaccharide) ,(CCH) phenylalanine, olefinic (protein assignment and polysaccharide), Proline, hydroxyproline, tyrosine , C-C stretching, proline (collagen assignment)			
918	Proline, hydroxyproline, Glycogen and lactic acid, C-C stretch of proline ring/glucose/lactic acid, C-C, praline ring (collagen assignment), Fatty acids	W	N/A	VW
937	Proline (collagen type I), Amino acid side chain vibrations of proline and hydroxyproline, as well as a (C-C) vibration of the collagen backbone, C-C backbone (collagen assignment), Glycogen, (C-C) residues (a-helix), C-C stretching, a-helix (proteins), C-O-C glycodides (carbohydrates), Proline, hydroxyproline, (C-C) skeletal of collagen backbone, C-C stretch backbone	M	N/A	W
1003	Phenylalanine, C-C skeletal	S	M	M
1033	Differences in collagen content, Phenylalanine mode, (CO), (CC), (CCO) (polysaccharides, pectin), C-H in-plan phenylalanine (proteins), Phenylalanine	W	N/A	N/A
1095	Lipid, Phosphodioxy, nucleic acids	W	N/A	N/A
1123	(C-C) skeletal of acyl backbone in lipid (transconformation), Heme ν(Cα-N) 1166(m)Vitamin A	M	M	W
1159	C-C/C-N stretching (proteins)	M	W	W
1164	Tyrosine (collagen type I) Tyrosine	W	N/A	N/A
1177	Cytosine, guanine	W	N/A	N/A
1207	Hydroxyproline, tyrosine (collagen assignment) Hydroxyproline, tyrosine (C-C6H5), tryptophan, phenylalanine (protein assignment) Vitamin A	W	N/A	N/A
1340	CH3, CH2 wagging (collagen assignment), Glucose, Proteins δ(CH2) 1366(w) Guanine/Tryptophan	M	N/A	W
1399	C55O symmetric stretch CH2 deformation	W	N/A	N/A
1450	CH2CH3 deformation, CH2CH3 deformation (collagen assignment), Protein bands, Umbrella mode of methoxyl, C-H bending mode of structural proteins, Collagen/Lipids/Proteins/ Phospholipids	S	W	W
1548	Tryptophan, (C55C), tryptophan (protein assignment), (C55C), porphyrin	W	VW	VW
1556	Tryptophan, (CN) and d(NH) amide II (protein assignment), (C55C) porphyrin, Tyrosine, amide II, COO2, Tryptophan	W	VW	VW
1579	Pyrimidine ring (nucleic acids) & heme protein	M	VW	VW
1662	Nucleic acid modes, Nucleic acid modes indicating the nucleic acid content in tissues, Lipids/Proteins	S	M	W
S-Strong, M- Medium, W-Weak, VW- Very Weak, P- Prominent, N/A- NotAvailable				

3.2 Protein Assignments

Three pairs of samples participated (CTR, VC and BPF), for each sample, three measurements were performed and the averaged spectrum was recorded. Spectra were preprocessed by baseline correction and area normalization[24]. Each sample was measuring three times and the averaged spectra used in further analysis. Fig 3a shows the average spectra of three groups of samples. Peaks of protein and collagen assignments a can be consistently observed in all three groups. At peak 623 – Adenine, 644 – (C-C), Wagging Tyrosine, 716 – Adenine/Tyrosine, 854 – ν(C-C), Proline δ(CCH) ring

breathing/Tyrosine, 937 – C – C Skeleton, Protein 1003 – C-C symmetric ring breathing, Phenylalanine, 1033 – δ(C-H), Phenylalanine, 1123 – ν(C-N) Protei,1340 – CH2 CH3 wagging Collagen , 1450 – δ(CH2), δ(CH3), Collagen, 1548 – ν(C=C) Tryptophen/ν(C=C)Porphyrin, 1579 –δ (C=C) Phenylalanine,1662 – ν(C=O) amide I, α-helix, Collagen

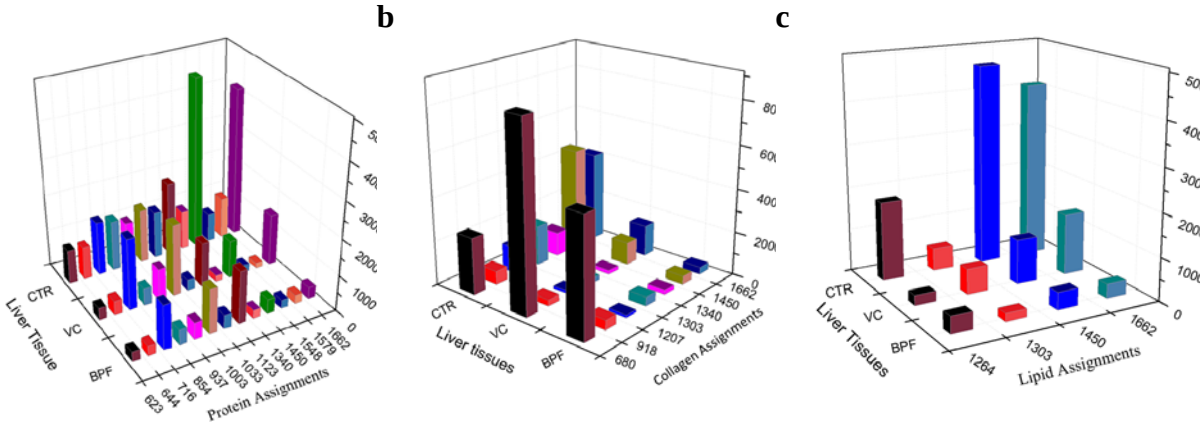

Figure 3 Cumulative Raman peak assignments for Protein (a), Collagen (b) and Lipid (c)

3.3 Collagen Assignments

Peaks of Collagen are the most distinct between groups 680 C-S stretching mode of cystine (collagen type I) (1), 918 collagen I (1), 1207 collagen assignment (1), 1303 Amide III (collagen I) (3), 1340 CH2 CH3 wagging Collagen (3), 1450 δ(CH2), δ(CH3), Collagen I, one of vibrational modes of collagen II (1), 1662 Alpha-Helix, collagen type IV (2) (Fig 3b).

3.4 Lipid Assignments

Lipids are undoubtedly one of the most important classes of biomolecule involved in the cellular signaling, energy storage and building of cellular membranes, In the present study Raman scattering cross section of several lipids signals is large due to the presence of long non-polar acyl chains in the structure, hence, bands assigned to lipids are omnipresent in the Raman spectra of the tissues [16]. The most characteristic features of Raman spectra of lipids are related to the presence of the hydrocarbon chain and for all lipids are observed in the three following regens 1500-1400, 1300-1250 and 1200-1050cm^{-1} in the fingerprint. The bands in the 1500-1400cm^{-1} range and around 1300cm^{-1} are assigned to scissoring and twisting vibrations of the CH2 and CH3 groups, respectively. Bands in the 1200-1500cm^{-1} regions are attributed to the C-C stretching vibrations. Additionally, very intense group of bands in the higher wavenumber range like 3100-2800 cm^{-1} are due to the C-H stretching modes are the characteristic feature of lipids spectra [25]. In the present study, Raman spectroscopy gave useful information on lipids, the spectra acquired with laser wavelength of 830nm (power of laser is 50mW) are generally ideal for most biological samples and including liver tissues. As mentioned Raman spectra collected with different laser lines can differ considerably depending on the polarization and orientation of crystal and macro-domains of the components. In summary upon lipids in this work can serve that each sample analyzed together with characteristic of the structure, function and properties, to this knowledge of lipids compositions on liver tissue and contents that Raman spectroscopy has a strong potential in the presented work. At 1264 fatty acids , 1303 Amide III (collagen assignment), 1450 one of vibrational modes of collagen , lipids, amino acids side chains of the proteins, 1662 Alpha-Helix, collagen [26] (Fig 3c).

4. Discussion

Three pairs of samples participated (CTR, VC and BPF) in our Raman microspectroscopy (Renishaw) investigations. The samples were irradiated at 830nm using He-Ne laser at an operating power of 50mW. Each sample was under radiation light for 10s. For each sample, three measurements were performed, of which the best signaling spectra was chosen and the spectra are shown altogether for

comparison. Separately every spectrum obtained was preprocessed by baseline correction and buffer subtraction before analysis. We have shown Raman spectra of the three groups of samples.

Strong peaks in CTR at Raman shift of 1003, 1452, 1662 cm^{-1} are observed. In comparison with the CTR, the corresponding peaks are medium in VC and BPF. These peaks can be evaluated more clearly with the intensity difference observed through spectroscopy (Table1).

Medium peaks in CTR at Raman shift of 680, 824, 854, 937, 1129, 1343, 1579 cm^{-1} are observed (Table1). In contrast to the CTR samples, liver tissue of VC at 680 shows strong intensity and of BPF shows very strong intensity. The intensity peak differences are evidently observed in the intensity Table in this document. This indicates that the VC and BPF absorbed more fructose and sucrose. The Raman shift for of VC and BPF at 1129 which is lipid transconformation medium and weak respectively. On assessing the intensity differences for Raman shift at 1129 CTR exhibits strong, BPF as medium and VC as weak peaks are observed. Whereas other Raman shifts are weakly or not observed in VC and BPF.

Weak peak intensities in CTR at Raman shift of 619, 636, 715, 918, 1033, 1095, 1159, 1164, 1177, 1207, 1399, 1552, 1556, 1739 cm^{-1} are acquired (Table1). When evaluated against CTR, liver tissue of VC at 715 observed medium intensity. The other Raman shifts for VC and BPF are observed but diminished and not visible. Comparisons of these Raman shifts are visibly classified in terms of strong, medium and weak with respect to CTR are shown in the peak intensity table in this document. In order to give better understanding of cumulative visibility of peaks and intensity differences of CTR, VC and BPF are shown in peak intensity differences Table.

In conclusion, the Raman spectrum of liver tissue of CTR, VC and BPF are observed. It contains the information about presence of biomolecules such as proteins, nucleic acids and lipids. In comparison with CTR (normal liver tissue treated with tap water), the intake of sugar in VC Liver tissue shows increase of band intensity at around 680 and $715cm^{-1}$, consequently the decrease of band intensity for BPF at 680 and $715cm^{-1}$ is caused by bergamot powder and may also be due to the metabolism within BPF treated liver tissue. The CTR peak at $1003cm^{-1}$ is the result of Phenylalanine (phy) collagen assignment and phy protein assignment, the decrease of this band intensity in VC and BPF may be caused by treatments undertaken. The peak at $1452cm^{-1}$ indicates protein bands umbrella mode of methoxyl observed in CTR, but we don't see umbrella behavior in the case of treated VC and BPF, instead it displays negative behavior. To note that the umbrella motion is totally symmetric and thus polarized in the Raman spectrum. The increase and decrease of other peaks are caused by amino acids, nucleic acids, lipids, collagen, proline, glucose etc. The intensity differences of liver tissue comparing with CTR (normal group) increased intensity with the increase in sugar and protein. This clearly shows that liver tissue with Raman spectra reflects more sugar and protein molecular component change in the blood caused by liver associated diseases [27]. And thus, the similarities with the increase in intensity peaks in the Raman spectra between liver tissues demonstrate that liver tissue follow same or slightly different pathology. Although, the peak increased intensities assigned to the same biomolecules but could undergo different metabolic.

In summary, we investigated the possibility of using Raman with Liver tissues of CTR, VC and BPF. The increased and decreased intensity peaks indicated that the biomolecule composition change in the liver tissue. The intensity increases of Raman peaks as a result of the deterioration of liver tissue in VC and BPF could be due to liver fibrosis. This preliminary research demonstrates the potential for the clinical use of liver tissue using Raman Spectroscopy. Further study will be focused on to determine by using the Surface enhanced Raman Scattering (SERS), in this way it is highly possible to obtain more enhanced peaks that are not visible (or diminished) in the Raman spectroscopy and also the inclusion of statistical analysis using large scale of samples [28-31].

Acknowledgments

The authors gratefully acknowledge “NUTRAMED – PON 03PE000_78” project for financial support. The authors also acknowledge the Department of Health Sciences for generously providing samples.

References

[1] H. Gilgenkrantz and A. Collin de l'Hortet, "Understanding Liver Regeneration: From Mechanisms to Regenerative Medicine," *Am J Pathol*, vol. 188, no. 6, pp. 1316-1327, Jun 2018, doi: 10.1016/j.ajpath.2018.03.008.

[2] G. Perozziello *et al.*, "Microfluidic device for continuous single cells analysis via Raman spectroscopy enhanced by integrated plasmonic nanodimers," *Opt Express*, vol. 24, no. 2, pp. A180-90, Jan 25 2016, doi: 10.1364/OE.24.00A180.

[3] M. L. Coluccio *et al.*, "Tailoring Chemometric Models on Blood-Derived Cultures Secretome to Assess Personalized Cancer Risk Score," *Cancers (Basel)*, vol. 12, no. 6, May 26 2020, doi: 10.3390/cancers12061362.

[4] M. G. Ramirez-Elias, E. S. Kolosovas-Machuca, D. Kershenobich, C. Guzman, G. Escobedo, and F. J. Gonzalez, "Evaluation of liver fibrosis using Raman spectroscopy and infrared thermography: A pilot study," *Photodiagnosis Photodyn Ther*, vol. 19, pp. 278-283, Sep 2017, doi: 10.1016/j.pdpdt.2017.07.009.

[5] M. Giarola *et al.*, "Fast and minimally invasive determination of the unsaturation index of white fat depots by micro-Raman spectroscopy," *Lipids*, vol. 46, no. 7, pp. 659-67, Jul 2011, doi: 10.1007/s11745-011-3567-8.

[6] M. L. Coluccio *et al.*, "Microfluidic platforms for cell cultures and investigations," *Microelectronic Engineering*, vol. 208, pp. 14-28, 2019/03/01/ 2019, doi: https://doi.org/10.1016/j.mee.2019.01.004.

[7] "<Raman_spectroscopy_explained_Renishaw.pdf>."

[8] G. Devitt, K. Howard, A. Mudher, and S. Mahajan, "Raman Spectroscopy: An Emerging Tool in Neurodegenerative Disease Research and Diagnosis," *ACS Chem Neurosci*, vol. 9, no. 3, pp. 404-420, Mar 21 2018, doi: 10.1021/acschemneuro.7b00413.

[9] T. Huser and J. Chan, "Raman spectroscopy for physiological investigations of tissues and cells," *Adv Drug Deliv Rev*, vol. 89, pp. 57-70, Jul 15 2015, doi: 10.1016/j.addr.2015.06.011.

[10] Y. Urasaki, C. Zhang, J. X. Cheng, and T. T. Le, "Quantitative Assessment of Liver Steatosis and Affected Pathways with Molecular Imaging and Proteomic Profiling," *Sci Rep*, vol. 8, no. 1, p. 3606, Feb 26 2018, doi: 10.1038/s41598-018-22082-6.

[11] O. Pickett-Blakely, K. Young, and R. M. Carr, "Micronutrients in Nonalcoholic Fatty Liver Disease Pathogenesis," *Cell Mol Gastroenterol Hepatol*, vol. 6, no. 4, pp. 451-462, 2018, doi: 10.1016/j.jcmgh.2018.07.004.

[12] G. Perozziello *et al.*, "Microfluidic Devices Modulate Tumor Cell Line Susceptibility to NK Cell Recognition," *Small (Weinheim an der Bergstrasse, Germany)*, vol. 8, pp. 2886-94, 09/24 2012, doi: 10.1002/smll.201200160.

[13] M. Z. Pacia, K. Czamara, M. Zebala, E. Kus, S. Chlopicki, and A. Kaczor, "Rapid diagnostics of liver steatosis by Raman spectroscopy via fiber optic probe: a pilot study," *Analyst*, vol. 143, no. 19, pp. 4723-4731, Sep 24 2018, doi: 10.1039/c8an00289d.

[14] B. G. Frushour and J. L. Koenig, "Raman scattering of collagen, gelatin, and elastin," *Biopolymers*, vol. 14, no. 2, pp. 379-91, Feb 1975, doi: 10.1002/bip.1975.360140211.

[15] M. M. McGee, O. Greengard, and W. E. Knox, "The quantitative determination of phenylalanine hydroxylase in rat tissues. Its developmental formation in liver," *Biochem J*, vol. 127, no. 4, pp. 669-74, May 1972, doi: 10.1042/bj1270669.

[16] K. Czamara, K. Majzner, M. Z. Pacia, K. Kochan, A. Kaczor, and M. Baranska, "Raman spectroscopy of lipids: a review," *Journal of Raman Spectroscopy*, vol. 46, no. 1, pp. 4-20, 2015, doi: https://doi.org/10.1002/jrs.4607.

[17] H. J. Morton and J. F. Morgan, "Studies on the dual requirement for phenylalanine and tyrosine in tissue cultures," *J Biol Chem*, vol. 234, pp. 2698-701, Oct 1959. [Online]. Available: https://www.ncbi.nlm.nih.gov/pubmed/14424463.

[18] X. Li, J. Lin, J. Ding, S. Wang, Q. Liu, and S. Qing, "Raman spectroscopy and fluorescence for the detection of liver cancer and abnormal liver tissue," *Conf Proc IEEE Eng Med Biol Soc*, vol. 2006, pp. 212-5, 2004, doi: 10.1109/IEMBS.2004.1403129.

[19] E. G. Fiona Lyng, Peter Gardner, "Preparation of tissues and cells for Infrared and Raman spectroscopy and Imaging," *Book Chapter 5*, 2011.

[20] C. Krafft, I. W. Schie, T. Meyer, M. Schmitt, and J. Popp, "Developments in spontaneous and coherent Raman scattering microscopic imaging for biomedical applications," *Chem Soc Rev*, vol. 45, no. 7, pp. 1819-49, Apr 7 2016, doi: 10.1039/c5cs00564g.

[21] F. Salomone, F. Galvano, and G. Li Volti, "Molecular Bases Underlying the Hepatoprotective Effects of Coffee," *Nutrients*, vol. 9, no. 1, Jan 23 2017, doi: 10.3390/nu9010085.

[22] J. De Gelder, K. De Gussem, P. Vandenabeele, and L. Moens, "Reference database of Raman spectra of biological molecules," *Journal of Raman Spectroscopy*, vol. 38, no. 9, pp. 1133-1147, 2007, doi: https://doi.org/10.1002/jrs.1734.

[23] "<Raman Spectroscopy for Analysis and Monitoring.pdf>."

[24] D. Nemecek, J. Stepanek, and G. J. Thomas, Jr., "Raman spectroscopy of proteins and nucleoproteins," *Curr Protoc Protein Sci*, vol. Chapter 17, p. Unit17 8, 2013, doi: 10.1002/0471140864.ps1708s71.

[25] K. Kochan, E. Maslak, C. Krafft, R. Kostogrys, S. Chlopicki, and M. Baranska, "Raman spectroscopy analysis of lipid droplets content, distribution and saturation level in Non-Alcoholic Fatty Liver Disease in mice," *J Biophotonics*, vol. 8, no. 7, pp. 597-609, Jul 2015, doi: 10.1002/jbio.201400077.

[26] K. Ilaslan, I. H. Boyaci, and A. Topcu, "Rapid analysis of glucose, fructose and sucrose contents of commercial soft drinks using Raman spectroscopy," *Food Control*, vol. 48, pp. 56-61, 2015/02/01/ 2015, doi: https://doi.org/10.1016/j.foodcont.2014.01.001.

[27] A. Asgharpour *et al.*, "A diet-induced animal model of non-alcoholic fatty liver disease and hepatocellular cancer," *J Hepatol*, vol. 65, no. 3, pp. 579-88, Sep 2016, doi: 10.1016/j.jhep.2016.05.005.

[28] C. Andreou *et al.*, "Imaging of Liver Tumors Using Surface-Enhanced Raman Scattering Nanoparticles," *ACS Nano*, vol. 10, no. 5, pp. 5015-26, May 24 2016, doi: 10.1021/acsnano.5b07200.

[29] X. Li *et al.*, "Noninvasive liver diseases detection based on serum surface enhanced Raman spectroscopy and statistical analysis," *Opt Express*, vol. 23, no. 14, pp. 18361-72, Jul 13 2015, doi: 10.1364/OE.23.018361.

[30] I. Valpapuram *et al.*, "Waveguiding and SERS Simplified Raman Spectroscopy on Biological Samples," *Biosensors (Basel)*, vol. 9, no. 1, Mar 3 2019, doi: 10.3390/bios9010037.

[31] G. Simone *et al.*, "A facile in situ microfluidic method for creating multivalent surfaces: Toward functional glycomics," *Lab on a chip*, vol. 12, pp. 1500-7, 03/09 2012, doi: 10.1039/c2lc21217j.